J Nanopart Res (2015) 17:322
DOI 10.1007/s11051-015-2887-7

RESEARCH PAPER

Photoelectrochemical water splitting under visible light over anti-photocorrosive In_2O_3-coupling ZnO nanorod arrays photoanode

Yan Zhang · Jinqiu Zhang · Mengyan Nie · Kai Sun · Chunhu Li · Jianqiang Yu

Received: 25 October 2014 / Accepted: 24 January 2015 / Published online: 28 July 2015

Abstract In_2O_3 quantum dots with a high crystallinity were deposited on the surface of ZnO nanorods through a chemistry bath method. The resulting In_2O_3-sensitizing ZnO nanorod arrays not only exhibited enhanced photoelectrochemical activity for water splitting under visible-light irradiation, but also possessed anti-photocorrosion property. The photo-induced charge-transfer property of In_2O_3 could be improved greatly by coupling with ZnO. This observation demonstrated that the heterojunction at the interface between In_2O_3 and ZnO could efficiently reduce the recombination of photo-induced electron–hole pairs and increase the lifetime of charge carriers and therefore enhance the photo-to-current efficiency of the In_2O_3–ZnO nanocrystalline arrays. It reveals that the heterojunction construction between two different semiconductors plays a very important role in determining the dynamic properties of their photo-generated charge carriers and their photo-to-current conversion efficiency.

Keywords In_2O_3 quantum dots · Photoelectrochemical water splitting · ZnO nanorod array · Thin-film photoanode

Electronic supplementary material The online version of this article (doi:10.1007/s11051-015-2887-7) contains supplementary material, which is available to authorized users.

Y. Zhang (✉) · C. Li
College of Chemistry and Chemical Engineering, Oceanology University of China, 238 Songling Road, Qingdao 266100, China
e-mail: zhangyanchem@qdu.edu.cn

Y. Zhang · J. Zhang · K. Sun · J. Yu
Faculty of Chemical Science and Engineering, Qingdao University, 308 Ningxia Road, Qingdao 266071, China

M. Nie
National Centre for Advanced Tribology at Southampton, School of Engineering Sciences, University of Southampton, Southampton SO17 1BJ, UK

J. Yu
Clean Energy Chemistry & Materials, Lanzhou Institute of Chemical Physics, CAS, Lanzhou, China

Introduction

Hydrogen is considered to be the most viable energy carrier for the future and its production at the present time is mainly derived from fossil fuels (Steinberg and Cheng 1989). Alternatively, photocatalytic and photoelectrochemical water splitting for hydrogen production offers a promising way for clean, low-cost, and environmentally friendly production of hydrogen by solar energy. Early work of photoelectrochemical hydrogen production was reported by Fujishima and Honda in 1972, who applied single-crystal TiO_2 semiconductor photoanode in the photocatalytic decomposition of water (Fujishima and Honda 1972). Subsequently, scientific and technical interests

in semiconductor photocatalysis have grown significantly. Currently, extensive studies in this area are mainly focused on inorganic n-type semiconductor materials with wide band gaps, such as TiO_2 (Fujishima and Honda 1972; Xiang et al. 2012; Ni et al. 2007; Hashimoto et al. 2005), $SrTiO_3$ (Iwashina and Kudo 2011), SnO_2 (Vinodgopal and Kamat 1995), $Sn_2Nb_2O_7$ (Zhou et al. 2013), and self-doped $K_4Nb_6O_{17}$.

Zinc oxide (ZnO) is a direct band gap semiconductor with energy gap of about 3.37 eV at room temperature. This material has been extensively studied in photoelectrochemical hydrogen production from water splitting (Wolcott et al. 2009; Maeda and Domen 2010; Liu et al. 2011; Maeda et al. 2005), photocatalytic degradation of organic pollutants (Daneshvar et al. 2004; Sakthivel et al. 2003; Ying et al. 2013; Mclaren et al. 2009; Wang et al. 2012), dye-sensitized solar cells (Luo et al. 2011; Li et al. 2012), photoluminescence materials (Pozina et al. 2010; Shana et al. 2005), gas sensing (Ahn et al. 2009; Navale et al. 2009), etc. Compared with TiO_2, which was the first semiconductor material applied in photoelectrochemical conversion, ZnO is considered as a suitable substitute for the application in photoelectrochemical water splitting and photoelectrochemical cells due to the similar energy-band structure with TiO_2 and high electron transfer rate (Fu et al. 2012; Sun et al. 2009).

However, one disadvantage of using ZnO photoanode for the photoelectrochemical splitting water to produce hydrogen is that the photo-to-current conversion efficiency should be further improved. Moreover, ZnO semiconductor suffers from the photo-induced dissolution, which greatly decreases its photocatalytic activity. The ultraviolet response properties also limit its further application in the area of hydrogen production. Therefore, semiconductor materials that respond to visible light with high efficiency must be developed to facilitate further application of this technology.

One-dimensional TiO_2 and ZnO nanotube (Zhang et al. 2014; Omar and Abdullah 2014; Sui et al. 2013; Li et al. 2012; Sun and Yan 2014; Moradian et al. 2014), nanorod (Liu et al. 2009; Lou and Chen 2014; Zhao et al. 2006; Yu et al. 2007), and nanobelt (Pan et al. 2013; Hu et al. 2012) array structures have recently been widely used in photoelectrochemical hydrogen production from water reduction. These semiconductor materials with a one-dimensional ordered nanostructure showed significantly better properties compared with disordered semiconductor nanoparticle film structures. Nanostructure semiconductor materials grown perpendicular to the conductive substrate can streamline the electron transfer pathways and effectively suppress charge recombination probability of photogenerated electrons and holes. Moreover, these nanostructures have a large specific surface area, which could provide a large number of loading sites for other semiconductor materials that respond to visible light. In addition, combining a semiconductor with a metal or coupling two different semiconductors to form a heterostructure is another way to promote the overall charge-transfer efficiency and to increase the lifetime of charge carriers (Li et al. 2014a; Jiang et al. 2011). Several types of materials have been investigated as semiconducting catalytic materials for photoelectrochemical hydrogen production. Especially, heterojunction semiconductors, which show good physical properties, e.g., semiconductor/semiconductor, metal oxide semiconductor/metal oxide semiconductor, semiconductor/metal, and metal oxide semiconductor/metal, core shell one-dimensional nanoheterostructures, have attracted great interest in photoelectrochemical process. The tailored nanostructure reduces the doping defects which can suppress the recombination of photogenerated charge carriers, resulting in an improved photocatalytic activity (Kargar et al. 2013).

Alternatively, researchers could use narrow band gap semiconductor materials in combination with these inert semiconductors and fabricated inorganic semiconductor quantum dot-sensitized visible-light-responsive photoelectrodes, such as CdS quantum dot-sensitized TiO_2 nanotube arrays (Li et al. 2014a), to provide metals with photoelectrochemical hydrogen production. Nevertheless, most of these narrow band gap quantum dots are unstable in ambient environments, and they could potentially trigger environmental pollution. Therefore, an environment friendly, and visible-light-responsive n-type semiconductor material with adequately negative conduction band potential must be developed to promote the applicability of this technology.

Indium oxide (In_2O_3) is one of the important transparent conducting oxides (TCOs) that are useful in applications such as gas sensor (Patel et al. 2003; Zhang and Zhang 2012), the indium-tin oxide (ITO) conductive glass (Ting et al. 2011), solar cells (Sun

and Ouyang 2012; Hu et al. 2011), photoelectric devices (Brinzari et al. 2010), liquid crystal displays (Park et al. 2009), etc. As an indirect band semiconductor with a direct band gap of 3.6 eV and an indirect band gap of 2.8 eV, In_2O_3 had also been used as an efficient narrow band gap semiconductor to couple with wide band gap semiconductor so as to extend the absorption spectra of the latter one from the UV region into the visible region. Recently, a variety of such kind of photocatalysts with heterostructure have been prepared, including nanoparticles, films, and so on. Because the band gap of In_2O_3 ($E_g = 2.8$ eV) is smaller than that of ZnO ($E_g = 3.2$ eV), but the conduction band (CB) of In_2O_3 (E_{CB} for $In_2O_3 = -0.63$ V versus NHE) is higher than that of ZnO (E_{CB} for ZnO $= -0.4$ V versus NHE), an efficient heterostructure between In_2O_3 and ZnO could be formed for the separation of photogenerated charge carriers. The formation of this structure favors for the separation of photo-induced electrons and holes and thus improved the photoelectrochemical efficiency of the heterostructure dramatically.

In the present work, ZnO arrays with relatively long nanorods were formatted on a Ti plate substrate by applying a hydrothermal method. Subsequently, In_2O_3 nanoparticles with relatively high crystallinity were deposited onto the ZnO nanorod surfaces using a chemistry bath method. It can be observed that ZnO nanorod arrays decorated with In_2O_3 could exhibit good anti-photocorrosion performance. The photo-induced charge-transfer property of In_2O_3 could also be improved greatly by coupling with ZnO. The heterojunction at the interface between In_2O_3 and ZnO could efficiently reduce the recombination of photo-induced electron–hole pairs to increase the lifetime of charge carriers and thus enhance the photo-to-current efficiency of the In_2O_3–ZnO nanocrystalline arrays.

Experimental section

Preparation of ZnO nanorod arrays

The preparation of ZnO on the Ti substrate was primarily based on the method used by Law et al. with minor modifications. First, a ZnO nanoparticle seed layer was deposited onto the Ti substrate (>99.6 % purity; 5 cm × 1 cm) by applying the following steps: 0.01 mol of zinc acetate and 0.012 mol of diethanolamine were dissolved in 25 mL anhydrous alcohol. A homogeneous sol was formed after 30 min of stirring at 60 °C. This sol was dispersed onto the Ti substrate by dip-coating method (1 cm min^{-1} pulling rate) to form a sol film. A uniform ZnO nanoparticle seed layer was formed after heating the sol film at 500 °C for 10 min. A total volume of 100 mL mixed solution containing 2.5 mmol of zinc acetate, 2.5 mmol of hexamethylene tetramine, and 0.6 mmol of polyethyleneimine was then prepared and stirred for 20 min in an ice bath. Subsequently, 80 mL of the above-mixed solution was transferred to a polytetrafluoroethylene tube with a total volume of 100 mL. The Ti plate prepared with a ZnO nanoparticle seed layer was immersed into the solution and faced down, maintained at a certain angle versus the tube wall, and hydrothermally reacted for 4 h at 95 °C. The prepared sample was repeatedly rinsed with deionized water and anhydrous alcohol. After that, it was annealed at 500 °C for 1 h. The hydrothermal reaction was repeated for one more time to increase the length of the ZnO nanorods. All reagents used in this study were analytical ones from licensed reagent companies.

Preparation of In_2O_3-sensitized ZnO photoanodes

The In_2O_3-sensitized ZnO nanorod arrays photoanode was prepared through the following steps: 0.15 mol L^{-1} of indium nitrate solution and 0.15 mol L^{-1} of citric acid solution were first prepared. The solution was refluxed for 3 h and rotary evaporated to form a wet sol state, which would be used as In_2O_3-precursor. The ZnO film was dipped into the precursor solution for 2 min, pulled slowly, rinsed, and dried. The films in this step repeated for once, twice, and triple times were denoted as ZnO–In_2O_3-1, ZnO–In_2O_3-2, and ZnO–In_2O_3-3, respectively. Then, all the samples were repeatedly rinsed with deionized water and anhydrous alcohol and hydrothermally grown at 150 °C for 3 h. Then copper wire was stuck using conductive silver tape and isolated with parafilms after the conductive silver tape was dried.

Characterizations of the thin film

The morphologies and the elemental compositions of the prepared photoelectrodes were analyzed using a

scanning electron microscope (SEM) (JSM-6700F; JEOL, Tokyo, Japan) with an energy dispersive spectrometer (EDS) (INCA Energy, OXFORD). The crystalline structures of the photoelectrodes were identified through X-ray diffraction (XRD) (D/MAX-2500/PC; Rigaku Co., Tokyo, Japan). The In_2O_3 distribution onto the ZnO nanorod surfaces, and the In_2O_3–ZnO interface bonding information were analyzed using a high-resolution transmission electron microscope (HRTEM, FEI Tecnai G20). The optical absorption properties of the photoelectrodes were investigated using a UV–Vis diffuse reflectance spectrophotometer (U-41000; HITACHI, Tokyo, Japan).

Photoelectrochemical measurements

A three-electrode system was employed to measure the photo-induced volt-ampere characteristic curve (I–V curve) and the variations of the photo-induced current density with time (I-t curve) of the prepared photoelectrodes using the CHI760C Electrochemical Workstation (Shanghai Chenhua Instrument Co., Ltd., Shanghai, China). The photoelectrodes (1 cm × 1 cm), Ag/AgCl, and platinum electrode acted as the working, reference, and counter electrodes, respectively. The electrolyte was 0.5 mol L^{-1} Na_2SO_4 solution. The I–V curves were measured from −1.5 to 1.0 V with a scanning rate of 0.05 V s^{-1}. The gap between the switching on and turning off of the light was 1 s. The I–t curves were measured at a 0 V bias potential. The white light source was a 300-W Xe arc lamp (PLS-SXE300, Beijing Changtuo Co. Ltd., Beijing, China) with an optical intensity of 265 mW cm^{-2}. A 420-nm cutoff filter was used to remove light with wavelengths less than 420 nm, ultimately generating visible light with an optical intensity of 200 mW cm^{-2}.

Results and discussions

Surface texture of ZnO NRA and In_2O_3-sensitized ZnO photoelectrodes

Figure 1 shows the SEM images of the ZnO NRA (a, b) as well as the In_2O_3-sensitized ZnO thin-film photoelectrodes after being hydrothermally grown for 1-3 times, respectively (c-h). From Fig. 1a and b, it can be seen that ZnO nanorods were grown evenly on the seed layer, and the rod length was approximately 4 μm. Longer nanorods could provide a larger number of loading sites for In_2O_3 deposition. The nanorod exhibited a regular hexagonal growth with a diameter of approximately 100 nm. The morphologies of various amount of In_2O_3-sensitized ZnO NRA are shown in Fig. 1c-h. It can be clearly observed that the surface of ZnO is not as smooth as that of pure ZnO NRA, and the rods increased its thickness. These observations indicated that In_2O_3 has been deposited onto the ZnO nanorod surface. Moreover, with the hydrothermally treatment time increasing from 1 to 3 times, In_2O_3 with large particles can be found forming on the surface of ZnO NRA.

TEM information

Figure 2 shows the HRTEM morphologies of the In_2O_3-sensitized ZnO for a second hydrothermal growth. It shows clearly from Fig. 2a that In_2O_3 nanoparticles were evenly distributed onto the ZnO nanorod surface. Moreover, the insert section suggested that the In_2O_3 nanoparticles with diameters of approximately 50 nm are homogeneously covered on the surface of the ZnO nanorods in a nearly single layer. This single layer resulted in the diameter of the nanorods increased to approximately 200 nm, which in agreement with the observed thickness increases in Fig. 1f. TEM and the corresponding high-resolution TEM (HRTEM) images of In_2O_3/ZnO NRA are shown in Fig. 2a and b. It is apparent that the ZnO nanorods are spindle shape rod with length of 2.5 μm. Lots of nanoparticle substances are attached on the surface of ZnO nanorods. The TEM microscopy of In_2O_3/ZnO NRA with high resolution in Fig. 2b showed two clearly crystalline domains with a uniform interplanar spacings of 0.25 nm and 0.29 nm. These values correspond to the {101} facet of ZnO and {222} facet of the orthorhombic In_2O_3 crystal, respectively. These observations demonstrated that the In_2O_3 grew along the {111} plane. Moreover, it is clear that the crystal interface between ZnO and In_2O_3 was closely combined, thus enabling the In_2O_3 photogenerated electrons to transfer swiftly onto the ZnO and consequently inhibiting the recombination and thus enhancing the separation efficiency of the photogenerated electrons and holes effectively.

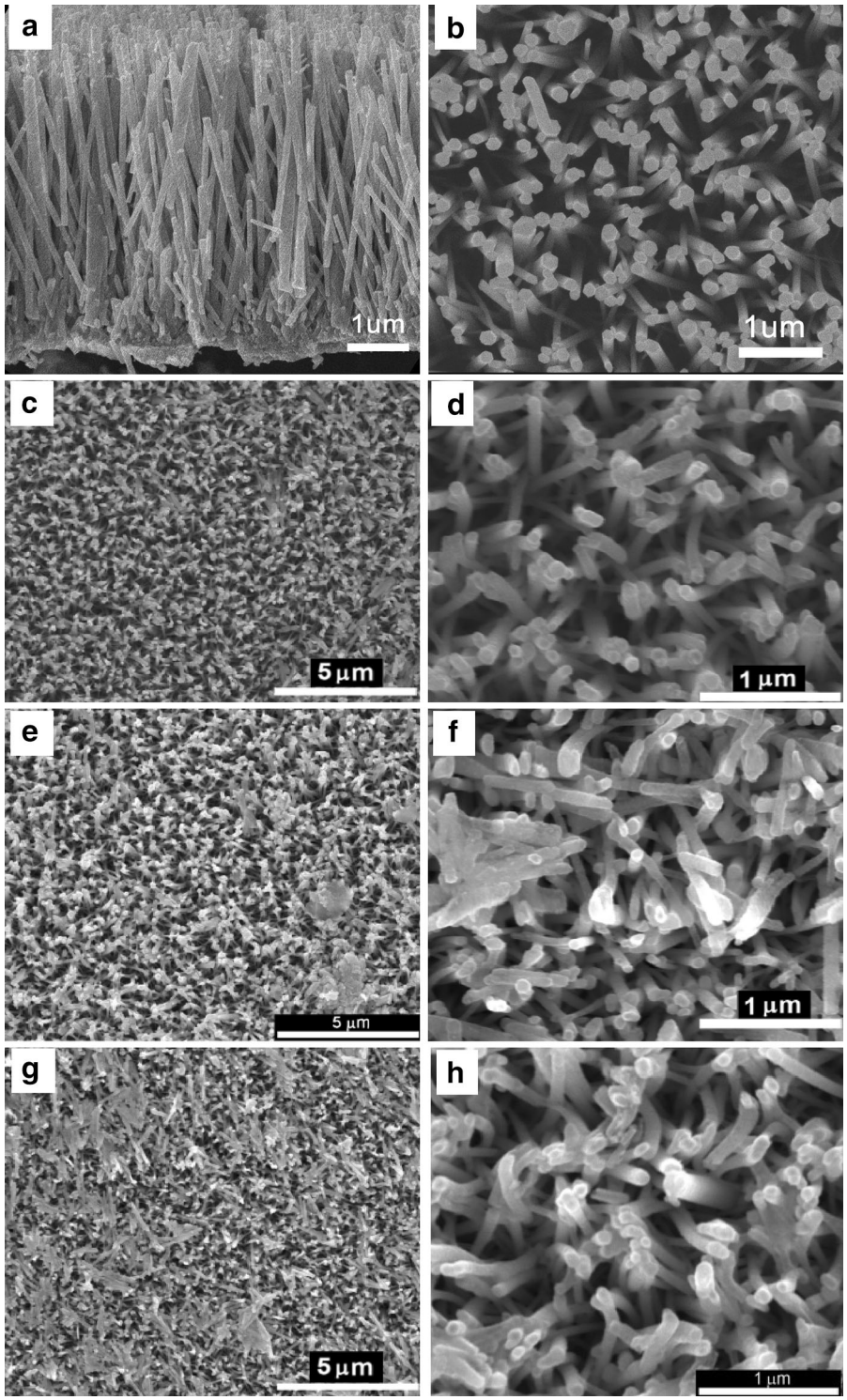

Fig. 1 SEM images of the ZnO thin-film photoelectrode (**a**, **b**) and In_2O_3-sensitized ZnO NRA after being hydrothermally grown once (**c**, **d**), twice (**e**, **f**), and three times (**g**, **h**)

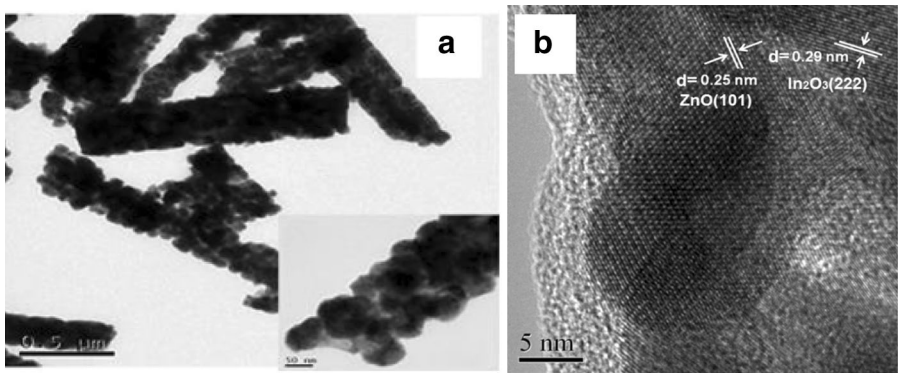

Fig. 2 HRTEM morphologies of the In_2O_3-sensitized ZnO NRA after being hydrothermally grown twice

Crystalline structure of ZnO and In_2O_3-sensitized ZnO

Figure 3 shows the XRD patterns of the ZnO NRA and In_2O_3-sensitized ZnO. The crystalline structure of the ZnO nanorod is similar to that of a wurtzite structure. A high-intensity diffraction peak was observed in the ZnO (002) crystal plane, revealing that the ZnO nanorod was grown in a high orientation along (002) direction. The In_2O_3 diffraction peak at $2\theta = 30.58°$ indicated that In_2O_3 existed on the surface of ZnO in a cubic structure, and the higher peak intensities of the In_2O_3 diffraction peaks indicated a relatively high crystallinity of the hydrothermally formatted In_2O_3.

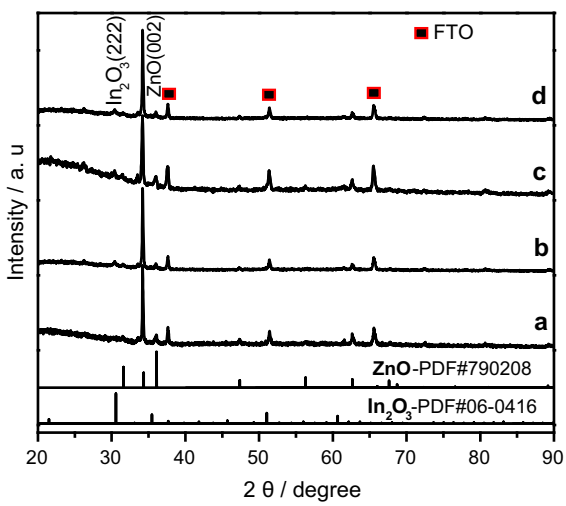

Fig. 3 The XRD patterns of cubic In_2O_3 PDF#06-0416, hexagonal ZnO PDF#79-0208, and *a* In_2O_3–ZnO nanorod *b* In_2O_3-ZnO-1 *c* In_2O_3–ZnO-2 *d* In_2O_3–ZnO-3

Photocorrosion suppression by surface hybridization of In_2O_3

To evaluate the photostability of ZnO NRA and In_2O_3-sensitized ZnO, the recycled experiments for the photocurrent density varied with respect to time over ZnO NRA and In_2O_3-sensitized ZnO photoelectrodes at a bias potential of 0.5 V under white light on and off in 0.5 mol/L of Na_2SO_4 solution were performed. The results are shown in Fig. 4. For ZnO photoelectrode, in the first cycle of light on and off, a strong photoresponse signal can be observed from curve a. The photocurrent density arrived to 1.75 mA/cm^2 at once when the light is turned on. Unfortunately, after another three cycles of light on and off, the photocurrent attenuates quickly to less than 0.25 mA/cm^2. This result suggests that ZnO photoelectrode is not stable; the photocorrosion resulted by the oxidation of photogenerated holes occurred seriously and reduced the photo-to-current conversion efficiency.

Interestingly, after ZnO NRA was surface hybridized with In_2O_3 layers, longer photoelectrochemical reaction does not affect the photocurrent density apparently. From curve b, c, and d, it can be found that although the initial photocurrent density decreases in a different degree with respective to pure-ZnO NRA, the photocurrents over In_2O_3-sensitized ZnO NRA photoelectrodes are sustained with a continues on and off. After 3 cycles of light on and off, the photocurrent density over both ZnO–In_2O_3-1 and ZnO–In_2O_3-2 photoelectrodes are more intensive than that of ZnO, demonstrating that the photocorrosion property of ZnO nanorod arrays has been suppressed by the sensitization of In_2O_3 quantum dots on the

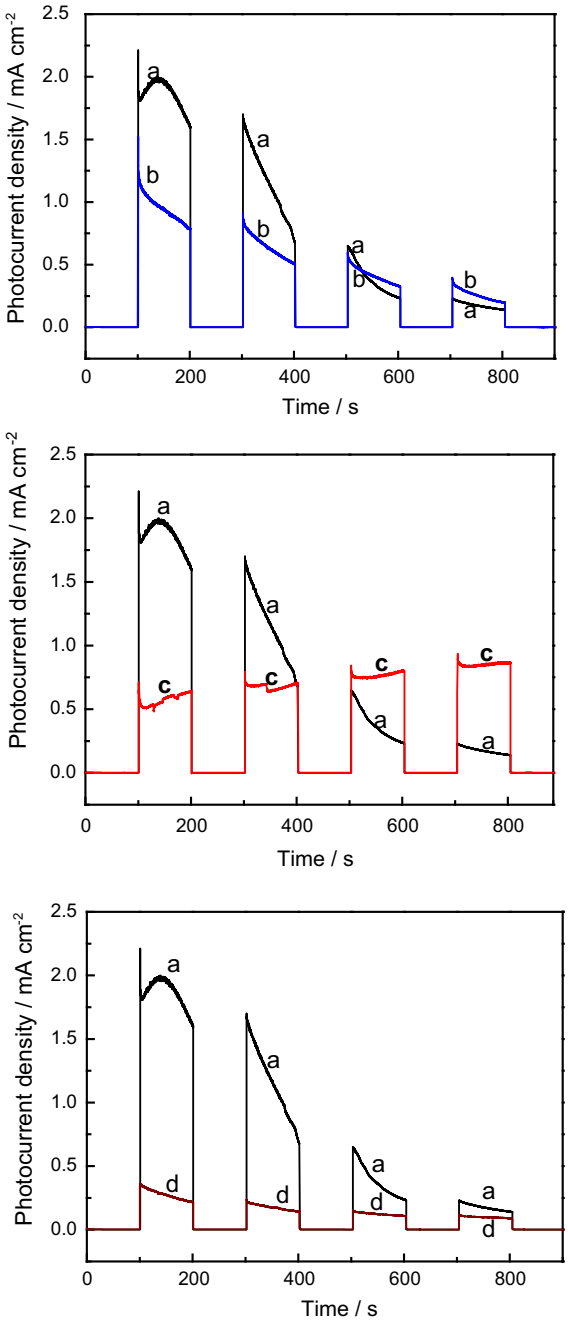

Fig. 4 Photocurrent versus potential curves for photoelectrode of *a* ZnO–In_2O_3-1, *b* ZnO–In_2O_3-2, *c* ZnO–In_2O_3-3 in the electrolyte of 0.5 mol L^{-1} of Na_2SO_4 solution with white light on and off

surface. The photocorrosion effect of ZnO was undoubtedly inhibited after surface hybridized by In_2O_3 nanoparticle layers.

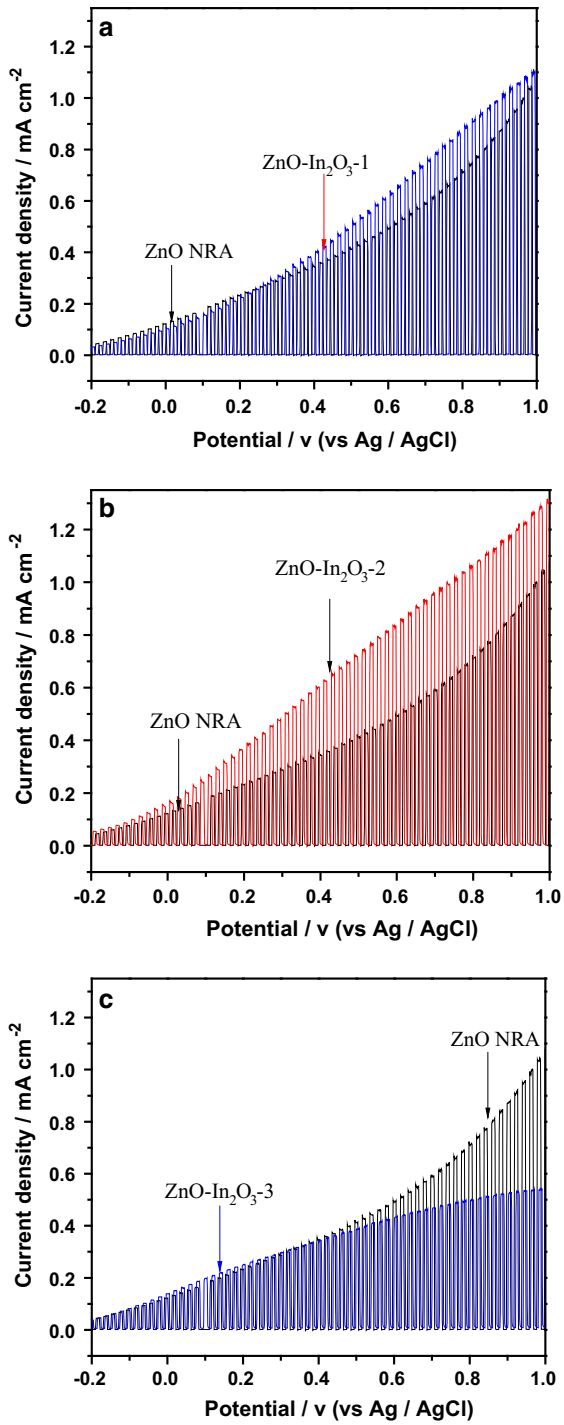

Fig. 5 Photocurrent density of different photoelectrodes under simulated sunlight. **a** ZnO nanorod **b** ZnO–In_2O_3-1, **b** ZnO–In_2O_3-2, **c** ZnO–In_2O_3-3

Enhanced photo-to-current conversion efficiency

Figure 5 shows photo-induced voltage ampere characteristic curve (J–V curve) over ZnO nanorod arrays and In_2O_3–ZnO composite photoelectrodes, respectively. From these two curves, the enhancement in the photo-to-current conversion efficiency of In_2O_3-sensitized ZnO composite photoelectrodes with respect to pure-ZnO NRA can be clearly observed. Moreover, according to the J–V curve of ZnO NRA, the onset potential of photo-induced current was generated at −0.5 V with respect to Ag/AgCl standard electrode. While the onset potential of the In_2O_3-sensitized ZnO composite photoelectrode negatively shifts to −0.6 V. The shift of the onset potential is attributed to the Fermi level of the In_2O_3–ZnO composite semiconductor negatively shifted. As we have known, the Fermi level of the n-type In_2O_3 is much closer to the conduction band potential than to the valence-band potential. When In_2O_3 was formatted on n-type ZnO NRA, the Fermi level potential of the composite photoelectrode will be negatively pulled to In_2O_3. Simultaneously, the flat-band potential will be negatively shifted and results in the negative shift of the photocurrent response potential. Moreover, the photogenerated current density of In_2O_3–ZnO composite photoelectrode increased significantly than that of ZnO NAR photoelectrode by the addition of In_2O_3. While the photo-induced current density increased with the bias voltage and a high value of 0.4 $mA.cm^{-2}$ is obtained when the bias voltage increases to 0.5 V. While the photogenerated current density of In_2O_3–ZnO NRA composite photo electrode is 0.75 mA cm^{-2}, almost twice greater than that of ZnO NRA photo electrode at the same bias voltage. This result can be attributed to the broadening of the light absorption range by In_2O_3 and to the promotion of the separation efficiency of the photogenerated electron–hole pairs by the formation of the interface electric field in the In_2O_3/ZnO interface.

The visible-light response of In_2O_3-sensitized ZnO

After being hydrothermally grown twice, the In_2O_3-sensitized ZnO NRA achieved an extremely high photo-to-current efficiency. However, we have also studied the photoelectron-chemical performance of the series of In_2O_3-sensitized ZnO NRA photoelectrodes under visible light for efficient solar energy utilization. Figure 6 shows the I-t curves obtained at a 0 V bias potential under visible light. For the photoelectrodes without In_2O_3, a negligible photo-induced current was generated, as shown in Curves 6a. The ZnO absorption wavelengths are known to be less than 380 nm, it cannot absorb visible light. This small photogenerated current density may be attributed to the inevitable faint UV light leakage from the light filter. Interestingly, the photo-induced current density of the In_2O_3-sensitized ZnO NRA that was hydrothermally grown twice reached 38 μA cm^{-2}. This result indicates that the majority of the photogenerated current was contributed by the visible-light absorption of the photoanodes. The In_2O_3-sensitized ZnO NRA that was hydrothermally grown twice can provide more loading sites for In_2O_3 quantum dots than hydrothermally grown only once. Therefore, the visible-light absorption of the former photoelectrodes is more complete than that of the latter. The photoelectrodes can thus generate high current density after UV light filtration.

The enhancement mechanism for photoelectrochemical property

It shows from above results that the In_2O_3-sensitized ZnO nanorod arrays not only exhibited enhanced photoelectrochemical hydrogen production activity under visible-light irradiation, but also possessed anti-photocorrosion property. Figure 7 depicts the

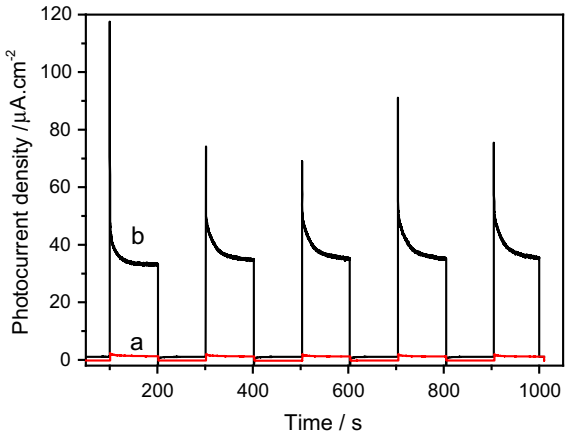

Fig. 6 Varations of the photo-induced current density with time of (*a*) ZnO NRA and (*b*) In_2O_3-sensitized ZnO NRA after being hydrothermally grown twice. All curves were obtained at 0 V bias potential under visible light on and off

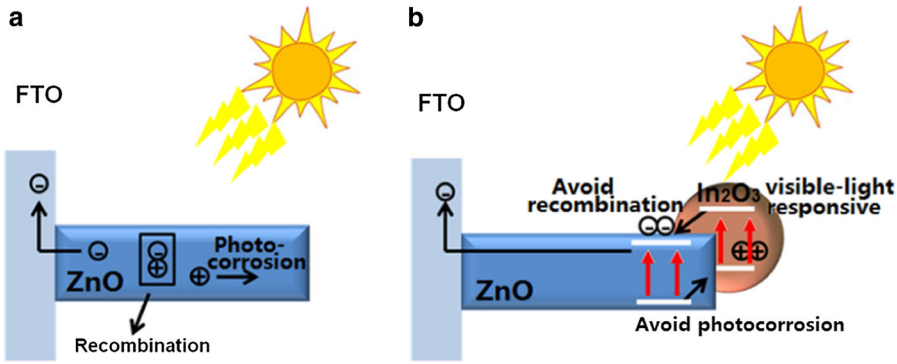

Fig. 7 **a** The photocorrosion of ZnO nanorod under white light. **b** The anti-photocorrosion of In_2O_3–ZnO nanorod under white light

photoelectrochemical process, including the charges separation, transfer, and recombination on ZnO nanorods and In_2O_3–ZnO under the irradiation of white light. From this picture, the inhibition of photocorrosion of ZnO by the encapsulate In_2O_3 and the enhancement of photo-to-current conversion efficiency by the sensitization of In_2O_3 can be clearly understood.

The photogenerated electrons will transfer along the photoelectrode to the counter electrode and produce the photocurrent, while the photogenerated holes will react with other species on the conduction band and result in the oxidation of ZnO. In the present study, the ZnO nanorods suffered serious photocorrosion during the photoelectrochemical process. Inevitably, the photoelectrochemical activity was significantly decreased, and even the morphology and composition of the nanoparticles varied. However, as the ZnO nanorod arrays were encapsulated with In_2O_3 nanoparticle layers, the photocorrosion was efficiently suppressed, and the stability was also significantly improved. The reasons are then proposed as follows.

For pure-ZnO thin film, most of the generated h^+ would participate in the reaction of photocorrosion, as shown in Fig. 7a. As the surface of ZnO was encapsulated by In_2O_3 nanoparticle layers, a more powerful n–n junction electric field was formed between In_2O_3 and ZnO, improving the transfer capacity of the photogenerated electrons and holes on the interface. Because the conduction band potential of In_2O_3 is more negative than that of ZnO, the photogenerated electrons can flow from the conduction band of In_2O_3 into that of ZnO, while the photogenerated holes may transfer to the conduction band of In_2O_3. Therefore, the In_2O_3 nanoparticle could gather the holes on the surface of ZnO, which would reduce the direct oxidation of ZnO with surface holes h^+ and thus suppress the serious photo-induced dissolution.

Furthermore, the n–n junction electric field formed between In_2O_3 and ZnO can also be used to explain the significant promotion of the photo-to-current performance of the In_2O_3-sensitized ZnO. The heterojunction thus efficiently facilitates the transfer of electrons mobility in In_2O_3 and increases the intensity of the interfacial electric field, thus exhibiting an efficient photoelectrochemical hydrogen production capacity from water reduction.

Conclusions

ZnO NRA with comparatively long nanorods was successfully prepared on a Ti substrate by applying a hydrothermal method twice. In_2O_3 nanoparticles with a high crystallinity and diameters of 50 nm were hydrothermally deposited as a compact and single layer onto the ZnO nanorod surface. In_2O_3-sensitized ZnO NRA could efficiently promote photogenerated electron mobility and increase the intensity of the interfacial electric field, thus exhibiting an efficient photoelectrochemical hydrogen production capacity from water reduction. The In_2O_3-sensitized ZnO NRA after being hydrothermally grown twice exhibits a potential application in photoelectrochemical hydrogen production from water reduction under sunlight.

Acknowledgement This work was financially supported by the financial supports from the National Foundation of Natural

Sciences (No.50878107 and No. 41206067). The China Postdoctoral Science Foundation (No. 214M551869) is also gratefully acknowledged.

References

Ahn MW, Park KS, Heo JH, Kim DW, Choi KJ, Park JG (2009) On-chip fabrication of ZnO-nanowire gas sensor with high gas sensitivity. Sens Actuators B Chem 138:168. doi:10.1016/j.snb.2009.02.008

Brinzari V, Lvanov M, Cho BK, Kamei M, Korotcenkov G (2010) Photoconductivity in In_2O_3 nanoscale thin films: interrelation with chemisorbed-type conductometric response towards oxygen. Sens Actuators B Chem 148:427. doi:10.1016/j.snb.2010.05.015

Daneshvar N, Salari D, Khataee AR (2004) Photocatalytic degradation of azo dye acid red 14 in water on ZnO as an alternative catalyst to TiO_2. J Photochem Photobiol A Chem 162:317. doi:10.1016/S1010-6030(03)00378-2

Fu DY, Han GY, Meng CF (2012) Size-controlled synthesis and photocatalytic degradation properties of nano-sized ZnO nanorods. Mater Lett 72:53. doi:10.1016/j.matlet.2011.12.047

Fujishima A, Honda K (1972) Electrochemical photolysis of water at a semiconductor electrode. Nature 238:37. doi:10.1038/238037a0

Han C, Yang MQ, Weng B, Xu YJ (2014) Improving the photocatalytic activity and anti-photocorrosion of semiconductor ZnO by coupling with versatile carbon. Phys Chem Chem Phys 16:16891. doi:10.1039/C4CP02189D

Hashimoto K, Irie H, Fujishima A (2005) TiO_2 Photocatalysis: a historical overview and future prospects. Jpn J Appl Phys 44:8269. doi:10.1143/jjap.44.8269

Hu ZY, Zhang JJ, Chen XL, Ren SR, Hao ZH, Geng XH, Zhao Y (2011) Performance of electron beam deposited tungsten doped indium oxide films as anodes in organic solar cells. Sol Energy Mater Sol Cells 95:2173. doi:10.1016/j.solmat.2011.03.020

Hu X, Heng B, Chen X (2012) Ultralong Porous ZnO nanobelt arrays grown directly on fluorine-doped SnO_2 substrate for dye-sensitized solar cells. J Power Sources 217:120. doi:10.1016/j.jpowsour.2012.06.004

Iwashina K, Kudo A (2011) Rh-Doped $SrTiO_3$ photocatalyst electrode showing cathodic photocurrent for water splitting under visible-light irradiation. J Am Chem Soc 133:13272. doi:10.1021/ja2050315

Jiang J, Zhang X, Sun PB, Zhang LZ (2011) ZnO/BiOI heterostructures: photoinduced charge-transfer property and enhanced visible-light photocatalytic activity. J Phys Chem C 115:20555. doi:10.1021/jp205925z

Kargar A, Jing Y, Kim ST, Riley CT, Pan X, Wang D (2013) ZnO/CuO heterojunction branched nanowires for photoelectrochemical hydrogen generation. ACS Nano 7:11112. doi:10.1021/nn404838n

Kudo A, Miseki Y (2009) Heterogeneous photocatalyst materials for water splitting. Chem Soc Rev 38:253. doi:10.1039/B800489G

Li Y, Zhang JW (2012) ZnO nanosheets derived from surfactant-directed process: growth mechanism, and application in dye-sensitized solar cells. J Am Ceram Soc 95:1241. doi:10.1111/j.1551-2916.2011.05030.x

Li L, Zhai T, Bando Y, Golberg D (2012) Recent progress of one-dimensional zno nanostructured solar cells. Nano Energy 1:91. doi:10.1016/j.nanoen.2011.10.005

Li JT, Cushing SK, Zheng P, Senty T, Meng F, Bristow AD, Manivannan A, Wu NQ (2014a) Solar hydrogen generation by a CdS-Au-TiO_2 sandwich nanorod array enhanced with Au nanoparticle as electron relay and plasmonic photosensitizer. J Am Chem Soc 136:8438. doi:10.1021/ja503508g

Li XD, Zhang ZM, Chen LL, Liu ZP, Cheng JL, Ni W, Xie EQ, Wang B (2014b) Cadmium sulfide quantum dots sensitized tin dioxide–titanium dioxide heterojunction for efficient photoelectrochemical hydrogen production. J Power Sources 269:866. doi:10.1016/j.jpowsour.2014.07.060

Liu ZF, Lei E, Ya J, Xin Y (2009) Growth of ZnO nanorods by aqueous solution method with electrodeposited ZnO Seed Layers. Appl Surf Sci 255:6415. doi:10.1016/j.apsusc.2009.02.030

Liu ZY, Bai HW, Xu SP, Sun DD (2011) Hierarchical CuO/ZnO "Corn-like" architecture for photocatalytic hydrogen generation. Int J Hydrog Energy 36:13473. doi:10.1016/j.ijhydene.2011.07.137

Lou YB, Chen JX (2014) Recent developments in one dimensional (1D) nanostructured TiO_2 for photoelectrochemical water splitting. Nanosci Nanotechnol Lett 6:361. doi:10.1166/nnl.2014.1781

Luo L, Tao W, Hu XY, Xiao T, Heng B, Huang W, Wang H, Han HW, Jiang Q, Wang JB, Tang YW (2011) Mesoporous F-doped ZnO prism arrays with significantly enhanced photovoltaic performance for dye-sensitized solar cells. J Power Sources 196:10518. doi:10.1016/j.jpowsour.2011.08.011

Maeda K, Domen K (2010) Solid solution of GaN and ZnO as a stable photocatalyst for overall water splitting under visible light. Chem Mater 22:612. doi:10.1021/cm901917a

Maeda K, Takata T, Hara M, Saito N, Inoue Y, Kobayashi H, Domen K (2005) GaN:ZnO solid solution as a photocatalyst for visible-light-driven overall water splitting. J Am Chem Soc 127:8286. doi:10.1021/ja0518777

Mclaren A, Valdes-Solis T, Li GQ, Tsang SC (2009) Shape and size effects of ZnO nanocrystals on photocatalytic activity. J Am Chem Soc 131:12540. doi:10.1021/ja9052703

Moradian R, Shahrokhi M, Amjaian S, Samadi J, Ijadi R (2014) Fe nanochain and nanowires encapsulation in isolated finite thickness zno nanotube and its bundle systems. Eur Phys J Appl Phys 67:20406. doi:10.1051/epjap/2014130441

Navale SC, Ravi V, Mulla IS (2009) Investigations on Ru Doped ZnO: strain calculations and gas sensing study. Sens Actuators B Chem 139:466. doi:10.1016/j.snb.2009.03.068

Ni M, Leung MK, Leung DY, Sumathy K (2007) A review and recent developments in photocatalytic water-splitting using TiO_2 for hydrogen production. Renew Sustain Energy Rev 11:401. doi:10.1016/j.rser.2005.01.009

Omar A, Abdullah H (2014) Electron transport analysis in zinc oxide-based dye-sensitized solar cells: a review. Renew Sustain Energy Rev 31:149–157. doi:10.1016/j.rser.2013.11.031

Pan K, Dong YZ, Zhou W, Pan QJ, Xie Y, Xie TF, Tian GH, Wang GF (2013) Facile fabrication of hierarchical TiO_2 Nanobelt/ZnO Nanorod heterogeneous nanostructure: an efficient photoanode for water splitting. ACS Appl Mater Interfaces 5:8314. doi:10.1021/am402154k

Park K, Sato W, Grause G, Kameda T, Yoshioka T (2009) Recovery of indium from In_2O_3 and liquid crystal display powder via a chloride volatilization process using polyvinyl chloride. Thermochim Acta 493:105. doi:10.1016/j.tca.2009.03.003

Patel NG, Patel PD, Vaishnav VS (2003) Indium tin oxide (ITO) thin film gas sensor for detection of methanol at room temperature. Sens Actuators B Chem 96:180. doi:10.1016/S0925-4005(03)00524-0

Pozina G, Yang LL, Zhao QX, Hultman L, Lagoudakis PG (2010) Size dependent carrier recombination in ZnO nanocrystals. Appl Phys Lett 97:131909. doi:10.1063/1.3494535

Sakthivel S, Neppolian B, Shankar MV (2003) Solar photocatalytic degradation of azo dye: comparison of photocatalytic efficiency of ZnO and TiO_2. Sol Energy Mater Sol Cells 77:65. doi:10.1016/S0927-0248(02)00255-6

Shana W, Walukiewicz W, Ager JW, Yu KM, Yuan HB, Xin HP, Cantwell G, Song JJ (2005) Nature of room-temperature photoluminescence in ZnO. Appl Phys Lett 86:191911. doi:10.1063/1.1923757

Steinberg M, Cheng HC (1989) Modern and prospective technologies for hydrogen production from fossil fuels. Int J Hydrog Energy 14:797. doi:10.1016/0360-3199(89)90018-9

Sui MR, Gong P, Gu XQ (2013) Review on one-dimensional ZnO nanostructures for electron field emitters. Front Optoelectron 6:386. doi:10.1007/s12200-013-0357-3

Sun K, Ouyang JY (2012) Polymer solar cells using chlorinated indium tin oxide electrodes with high work function as the anode. Sol Energy Mater Sol Cells 96:238. doi:10.1016/j.solmat.2011.10.002

Sun Y, Yan KP (2014) Effect of anodization voltage on performance of TiO_2 nanotube arrays for hydrogen generation in a two-compartment photoelectrochemical cell. Int J Hydrog Energy 39:11368. doi:10.1016/j.ijhydene.2014.05.115

Sun JH, Dong SY, Wang YK, Sun SP (2009) Preparation and photocatalytic property of a novel dumbbell-shaped ZnO microcrystal photocatalyst. J Hazard Mater 172:1520. doi:10.1016/j.jhazmat.2009.08.022

Ting CC, Cheng WL, Lin GC (2011) Structural and opto-electrical properties of the tin-doped indium oxide thin films fabricated by the wet chemical method with different indium starting materials. Thin Solid Films 519:4286. doi:10.1016/j.tsf.2011.02.004

Vinodgopal K, Kamat PV (1995) Enhanced rates of photocatalytic degradation of an azo dye using SnO_2/TiO_2 coupled semiconductor thin films. Sci Technol 29:841. doi:10.1021/es00003a037

Wang X, Liao MR, Zhong YT, Zheng JY, Tian W, Zhai TY, Zhi CY, Ma Y, Yao JN, Bando Y, Golberg D (2012) ZnO hollow spheres with double-yolk egg structure for high-performance photocatalysts and photodetectors. Adv Mater 24:3421. doi:10.1002/adma.201201139

Wolcott A, Smith WA, Kuykendall TR (2009) Photoelectrochemical study of nanostructured ZnO thin films for hydrogen generation from water splitting. Adv Funct Mater 19:1849. doi:10.1002/adfm.200801363

Xi Y, Wu WZ, Fang H, Hu CG (2012) Integrated ZnO nanotube arrays as efficient dye-sensitized solar cells. J Alloy Compd 529:163. doi:10.1016/j.jallcom.2012.02.183

Xiang QJ, Yu JG, Jaroniec M (2012) Synergetic effect of MoS_2 and graphene as cocatalysts for enhanced photocatalytic H_2 production activity of TiO_2 nanoparticles. J Am Chem Soc 134:6575. doi:10.1021/ja302846n

Ying YL, Song T, Huang HW, Peng XS (2013) Nanoporous ZnO nanostructures for photocatalytic degradation of organic pollutants. Appl Phys A 110:351. doi:10.1007/s00339-012-7273-z

Yu K, Jin ZG, Liu XX, Liu ZF, Fu YN (2007) Synthesis of Size-tunable ZnO nanorod arrays from $NH_3{\cdot}H_2O/Zn(NO_3)_2$ solutions. Mater Lett 61:2775. doi:10.1016/j.matlet.2006.10.029

Zhang WH, Zhang WD (2012) Biomolecule-assisted synthesis and gas-sensing properties of porous nanosheet-based corundum In_2O_3 microflowers. J Solid State Chem 186:29. doi:10.1016/j.jssc.2011.11.031

Zhang YQ, Heng LP, Jiang L (2014) Chemically controllable fabrication of one-dimensional ZnO nanostructures and their applications in solar cells. J Nanosci Nanotechnol 14:5597. doi:10.1166/jnn.2014.8862

Zhao J, Jin ZG, Li T, Liu XX, Liu ZF (2006) Growth of ZnO Nanorods by the chemical solution method with assisted electrical field. J Am Ceram Soc 89:2654. doi:10.1111/j.1551-2916.2006.01103.x

Zhou M, Lou XW, Xie Y (2013) Two-dimensional nanosheets for photoelectrochemical water splitting: possibilities and opportunities. Nano Today 8:598. doi:10.1016/j.nantod.2013.12.002